Microseism Noise in the Philippine Sea

Stephen, R.A. (WHOI), Bromirski, P.D. (SIO), Gerstoft, P. (SIO) and Worcester, P.F. (SIO)

Abstract

Microseism noise, generated by wave-wave interaction of ocean surface gravity waves and peaking near 0.25Hz, is the largest amplitude, continuous (acceleration) vibration on earth in the seismic band from 0.0001 to 10Hz. Although microseisms have been studied extensively over the past seventy years, significant issues remain regarding their excitation and propagation. In a recent paper Bromirski et al (JGR, 2013) point out that there is an important distinction between microseisms generated in deep and shallow water. Most microseisms observed on continents are generated in shallow water near coastlines. Microseisms generated in deep water are observed on seafloor sensors but do not transition readily to continents. The Ocean Bottom Seismometer Augmentation to the Philippine Sea (OBSAPS) Experiment has provided a unique opportunity to study the excitation and propagation of microseism noise (from 0.05 to 1.0Hz) in the oceans by combining ocean bottom seismometer observations with co-located and simultaneous observations of the acoustic field in the ocean. The depth dependence of the acoustic field in the ocean can be used to distinguish between Rayleigh waves, acoustic and elastic pseudo-Rayleigh waves, and ocean acoustic modes as propagation mechanisms for microseism energy. (OBSAPS experiment was funded by ONR.)

I. Background - Pseudo-Rayleigh Waves (pRg)

In marine seismology the physics of wave propagation for the double frequency microseism band (0.1-0.5Hz) and typical ocean depths (100-6000m) spans the transition between solid earth seismology and ocean acoustics. At microseism frequencies, the water wavelengths are much longer than the thickness of soft sediment layers on the seafloor, the seafloor sediments can be ignored, and the bottom can be considered to consist of "hard rock", with a shear speed greater than the sound speed in the water. For laterally homogeneous models, the different phases generated by ocean surface gravity waves were reviewed by Ardhuin and Herbers (2012).

Many papers on microseism generation assume that, because storms at sea excite "Rayleigh waves" and because land arrays observe "Rayleigh waves", then Rayleigh waves must easily propagate from the deep ocean onto land. Bromirski et al (2013) point out that storms at sea excite "pseudo-Rayleigh waves", which are significantly different from "Rayleigh waves", through the microseism band (0.1-0.5Hz) (Figure 1). For example, at frequencies above 0.2Hz and a water depth of 5000m "pseudo-Rayleigh waves" have considerable energy in the water column and propagate at water sound speeds (see Figure 2 for the frequency-depth trade-off of phase speed).

Pseudo-Rayleigh waves (below a fluid layer) do become indistinguishable from Rayleigh waves (on land) at low frequencies (below about 0.1Hz) where the thickness of the fluid layer becomes small compared to an acoustic wavelength. But for microseism studies the band of interest, 0.1-0.5Hz, spans the transition from free surface Rayleigh waves to propagating acoustic modes, acoustic pseudo-Rayleigh waves and direct water waves in the ocean as the ocean thickens with respect to frequency.

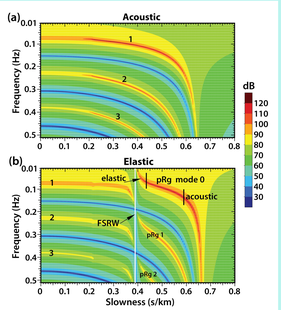

Figure 1: The magnitude of the wave fields in frequency-slowness space for a fluid layer (5 km thick with a sound speed of 1.520 km/s and a density of 1 kg/m^3) over (a) a fluid half-space (isoacoustic, zero shear modulus, with sound speed of 4.730 km/s and density of 3 kg/m^3), and (b) a solid half-space (elastic, compressional, and shear speeds of 4.730 and 2.800 km/s, respectively, free surface Rayleigh wave (FSRW) speed of 2.565 km/s, and a density of 3 kg/m^3). The FSRW slowness (0.39 s/km, white line) is the lower slowness bound for pseudo- Rayleigh wave (pRg) modes. Approximate boundaries where fundamental pRg mode 0 exhibits predominantly elastic or acoustic behavior are indicated by vertical black lines, with a transition region between. Acoustic modes 1, 2, and 3 are common to a and b. Although the fluid halfspace in a is unrealistic, comparison of these cases shows the effect of shear. Source and receivers are 0.050 km above the interface. These plots were computed using a seismo-acoustic fast-field algorithm (Schmidt, 1988). [Figure from Bromirski et al (2013).]

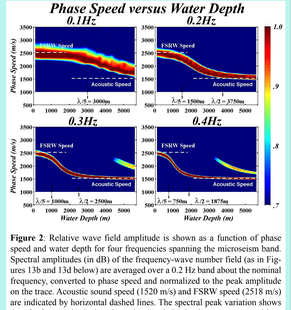

Figure 2: Relative wave field amplitude is shown as a function of phase speed and water depth for four frequencies spanning the microseism band. Spectral amplitudes (in dB) of the frequency-wave number field (as in Figures 13b and 13d below) are averaged over a 0.2 Hz band about the nominal frequency, converted to phase speed and normalized to the peak amplitude on the trace. Acoustic sound speed (1520 m/s) and FSRW speed (2518 m/s) are indicated by horizontal dashed lines. The spectral peak variation shows that, for frequencies in the microseism band, the dominant energy transitions from FSRW speeds to acoustic speeds as water depth increases. Phase-speed resolution, indicated by the width of the speetral peak, improves with increasing frequency. pRg mode 1 (see Figure 1) becomes evident between FSRW and acoustic phase speeds at deeper water depths as frequency increases. [Figure from Bromirski et al].

II. The OBSAPS Experiment

The OBSAPS cruise sailed Kaohsiung to Kaohsiung, April 29 to May 16, 2011. A fifteen element OBSAPS - Distributed Vertical Line Array (O-DVLA) with hydrophone modules from 12 to 852m above the seafloor was deployed in the Philippine Sea near 21degN, 126degE (Figure 3). Four short-period Ocean Bottom Seismometers (OBSs) and two long-period OBSs were deployed at 2km range from the O-DVLA (Figures 4 & 5). All of the OBSs had three-component inertial sensors and an acoustic pressure sensor. Three of the short period OBSs also had an external, autonomously recording hydrophone module identical to the hydrophone modules on the O-DVLA. Data from nearby continental and island Global Seismic Network (GSN) stations (Figure 6) can be used to study the similarities and differences in microseisms with the seafloor station. The data acquisition interval included about a week of calm conditions with wind speeds of less than 5 to 10knots (Figure 7). Following this, Tropical Storm AERE grew to the Southeast of the site and eventually tracked almost directly over the site (Figure 3) with observed wind speeds of almost 50knots.

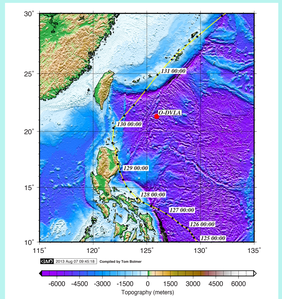

Figure 3: Location of the OBSAPS experiment (red dot) and the track of Tropical Storm AERE.

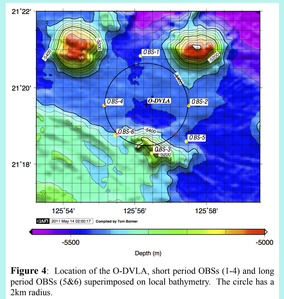

Figure 4: Location of the O-DVLA, short period OBSs (1-4) and long period OBSs (5&6) superimposed on local bathymetry. The circle has a 2km radius.

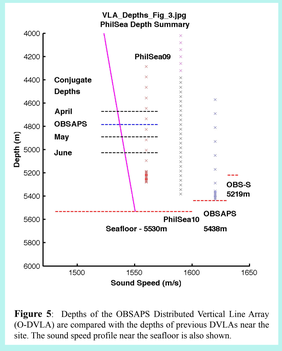

Figure 5: Depths of the OBSAPS Distributed Vertical Line Array (O-DVLA) are compared with the depths of previous DVLAs near the site. The sound speed profile near the seafloor is also shown.

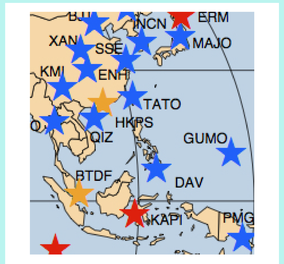

Figure 6: Detail of the GSN station map showing the island and continental GSN stations in the vicinity of the OBSAPS array.

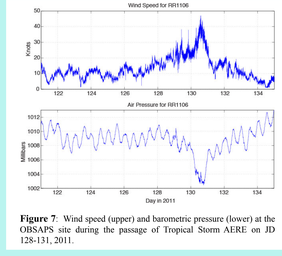

Figure 7: Wind speed (upper) and barometric pressure (lower) at the OBSAPS site during the passage of Tropical Storm AERE on JD 128-131, 2011.

III. The Data

Traditionally, tropical cyclones, like AERE, are a strong source of microseism energy. Spectrograms of the hydrophone module data (eg Figure 8) and OBS vertical component data (eg Figure 9) show examples of both distant (on JD 124) and local (JD127-132) microseism sources. The hydrophone modules were designed for use above 10Hz but they still resolve the double frequency microseisms (0.12 to 1.0Hz, Figure 10). The long period seismometers (Trillium 240s) provide valid data down to 0.02Hz and under quiet conditions resolve the primary microseisms at 0.06Hz in both vertical and horizontal components (Figure 11). The O-DVLA provides the first opportunity to observe the depth dependence of microseism noise in the ocean directly above an array of OBSs (Figure 12).

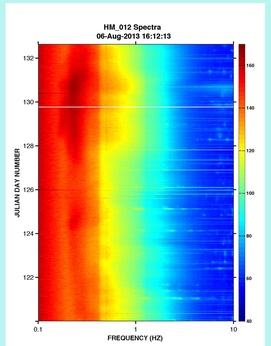

Figure 8: Spectrogram for the hydrophone module 12m off the seafloor on the O-DVLA. Color bar has units of dB re: microPa^2/Hz.

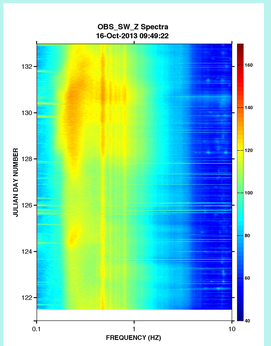

Figure 9: Spectrogram for the vertical component of the long period OBS (OBS5 in Figure 4). Color bar units minus 243.5dB, the acoustic impedance (Stephen et al., 2013), are re: (m/s)^2/Hz.

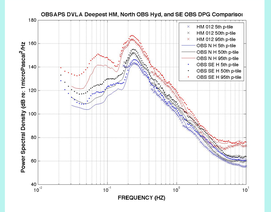

Figure 10: 5th, 50th and 95th percentile spectra for the hydrophone module at 12m on the O-DVLA, for the OBSIP hydrophone on the North short-period OBS, and for the differential pressure gauge on the Southeast long-period OBS.

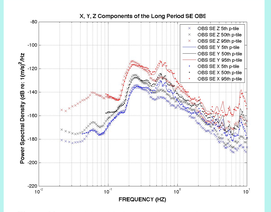

Figure 11: 5th, 50th and 95th percentile spectra for the X, Y and Z inertial sensors on the Southeast long-period OBS.

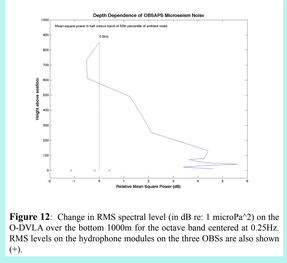

Figure 12: Change in RMS spectral level (in dB re: 1 microPa^2) on the O-DVLA over the bottom 1000m for the octave band centered at 0.25Hz. RMS levels on the hydrophone modules on the three OBSs are also shown (+).

IV. The Modeling

TDFD modeling has been carried out to confirm the hypothesis that double-frequency microseisms excited over the deep ocean propagate well in the deep ocean but do not readily propagate onto continents (Bromirski et al., 2005; Bromirski et al., 2013; Latham and Sutton, 1966). There are three aspects to this. First, shallow pressure sources, like wave-wave interaction, put more energy into acoustic modes and acoustic pseudo-Rayleigh waves in deep water and than in shallow water (Figure 13). Second, something about the ocean-continent transition (distinct from ocean-island transitions) strongly attenuates deep-water generated microseisms so that they do not readily transition onto continents (see the test examples in Figures 14 and 15). Third, there is something about deep water propagation per se, for example scattering from bathymetric roughness, that attenuates deep-water generated microseisms, but not necessarily shallow-water generated microseisms.

Figure 13 demonstrates the dramatic difference of excitation and propagation between shallow (100m) and deep (5,000) water. For the 100 m thick ocean (Figure 13, top), the water is sufficiently thin with respect to any wavelengths at the source frequencies that this is essentially a free-surface problem. For the 5,000m thick ocean (Figure 13, bottom) most of the energy goes into acoustic and acoustic pseudo-Rayleigh modes (pRg0 and pRg1, see Figure 1) that travel at the water phase speed. Relatively little energy travels at the free surface Rayleigh wave speed (FSRW).

Two test examples are shown to demonstrate 2-D TDFD results for ocean-continent transitions. Figure 14 shows a calculation for a point, compressional source in shallow (100m) water propagating onto land. Elastic pseudo-Rayleigh waves are excited in shallow water and these transition easily into free-surface Rayleigh waves (FSRW) on land. Figure 15 shows a similar set of plots for deep-water excitation. The time series for deep-water receivers (left side of the upper left panel) show the same acoustic pseudo-Rayleigh waves as in Figure 13d. These reflect strongly from the ocean-shelf boundary sending similar acoustic pseudo-Rayleigh waves back into deep water. A small amount of each component of acoustic pRg does convert to FSRW on land.

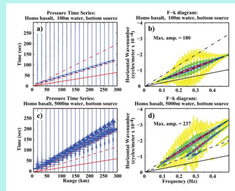

Figure 13: Pressure time series and frequency-wavenumber plots for shallow (100m, a&b) and deep (5,000m, c&d) water over a homogeneous, solid half-space. In shallow water only the free-surface Rayleigh wave (---, FSRW, or elastic pseudo-Rayleigh wave) is excited. In deep water, acoustic pRg0 (-·-·-, or acoustic pseudo-Rayleigh wave), pRg1 and even a little pRg2 are excited.

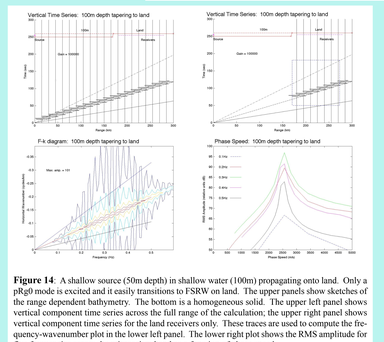

Figure 14: A shallow source (50m depth) in shallow water (100m) propagating onto land. Only a pRg0 mode is excited and it easily transitions to FSRW on land. The upper panels show sketches of the range dependent bathymetry. The bottom is a homogeneous solid. The upper left panel shows vertical component time series across the full range of the calculation; the upper right panel shows vertical component time series for the land receivers only. These traces are used to compute the frequency-wavenumber plot in the lower left panel. The lower right plot shows the RMS amplitude for five frequencies across the microseism band as a function of phase speed.

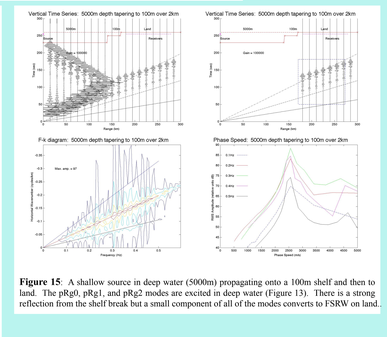

Figure 15: A shallow source in deep water (5000m) propagating onto a 100m shelf and then to land. The pRg0, pRg1, and pRg2 modes are excited in deep water (Figure 13). There is a strong reflection from the shelf break but a small component of all of the modes converts to FSRW on land.

V. Conclusions

Over the microseism band (0.1-0.5Hz), wave-wave interaction excites a different set of modes in shallow (~100m) and deep (~5,000) water. Wave-wave interaction in shallow water excites fundamental surface Rayleigh waves (FSRW) that propagate easily onto continents. Wave-wave interaction in deep water excites little FSRW and puts most of its energy into acoustic modes and acoustic pseudo-Rayleigh waves that do not transition easily onto continents.

The 2011 OBSAPS experiment in the Philippine Sea deployed an array of ocean bottom seismometers beneath a vertical line array of hydrophones in the water column. This is a unique opportunity to simultaneously observe acoustic modes in the ocean and interface waves on the seafloor for microseisms generated by a passing tropical cyclone.

REFERENCES

Ardhuin, F., Balanche, A., Stutzmann, E., and Obrebski, M. (2012), "From seismic noise to ocean wave parameters: general methods and validation," J. Geophys. Res. 117, 1-19.

Bromirski, P. D., Duennebier , F. K., and Stephen, R. A. (2005). "Mid-ocean microseisms," Geochem. Geophys. Geosys. 6, doi:10.1029/2004GC000768.

Bromirski, P. D., Stephen, R. A., and Gerstoft, P. (2013). "Are deep-ocean-generated surface-wave microseisms observed on land?," J. Geophys. Res. 118, 1-20.

Brooks, L. A., Townsend, J., Gerstoft, P., Bannister, S., and Carter, L. (2009). "Fundamental and higher-mode Rayleigh wave characteristics of ambient noise in new Zealand," Geophys. Res. Lett. 36.

Cao, S., and Muirhead, K. J. (1993). "Finite difference modeling of Lg blockage," Geophys. J. Int. 116, 85-96.

Ewing, W. M., Jardetzky, W. S., and Press, F. (1957). Elastic waves in layered media, (McGraw-Hill Book Company, Inc., New York), pp.

Gerstoft, P., Shearer, P. M., Harmon, N., and Zhang, J. (2008). "Global P, PP, PKP wave microseisms observed from distant storms," Geophys. Res. Lett. 35, L23306.

Harmon, N., Forsyth, D., and Webb, S. (2007). "Using ambient seismic noise to determine short-period velocities and shallow shear velocities in young oceanic crust," Bull. Seismol. Soc. Am. 97, 2009-2023.

Haubrich, R. (1963). "A statistical analysis of the generation of microseisms," Rev. Geophys. 1, 177-210.

Haubrich, R. A., and McCamy, K. (1969). "Microseisms: coastal and pelagic sources," Rev. Geophys. 7, 539-571.

Lacoss, R. T., Kelly, E. J., and Toksoz, M. N. (1969). "Estimation of seismic noise structure using arrays," Geophysics 34, 21-38.

Latham, G. V., and Sutton, G. H. (1966). "Seismic measurements on the ocean floor - 1. Bermuda area," J. Geophys. Res. 71, 2545-2573.

Lee, A. W. (1935). "On the direction and approach of microseismic waves," Proceedings of the Royal Society of London, Series A, Mathematical and Physical Sciences 149, 183-199.

National Research Council (1953). Symposium on Microseisms, Publ. 306, , Washington, D.C., pp.

Pontificia Academia Scientiarum (1952). "La semaine d'étude sur le problème des microséismes " Pontif. Acad. Sci. Scripta Varia 12.

Schmidt, H. (1988), SAFARI, Seismo-acoustic fast field algorithm for range-independent environments, User's Guide, (SACLANT Undersea Research Centre).

Stephen, R. A., Bolmer, S. T., Udovydchenkov, I. A., Dzieciuch, M. A., Worcester, P. F., Andrew, R. K., Mercer, J. A., Colosi, J. A., and Howe, B. M. (2013). "Deep seafloor arrivals in long range ocean acoustic propagation," J. Acoust. Soc. Am. 134, 3307-3317.

Tanimoto, T., and Ishimaru, S. (2006). "Seasonality in particle motion of microseisms," Geophys. J. Int. 166, 253-266.

Yao, H., Gouedard, P., Collins, J. A., McGuire, J. J., and van der Hilst, R. D. (2011). "Structure of young East Pacific Rise lithosphere from ambient noise correlation analysis of fundamental- and higher-mode Scholte-Rayleigh waves," Comptes Rendus Geoscience 343, 571-583.

Zhang, J., Gerstoft, P., and Bromirski, P. D. (2010). "Pelagic and coastal sources of P-wave microseisms: generation under tropical cyclones," Geophys. Res. Lett. 37, L15301.

Zhang, T.-R., and Lay, T. (1995). "Why the Lg phase does not traverse oceanic crust," Bull. Seismol. Soc. Am. 85, 1665-1678.

Abstract

Microseism noise, generated by wave-wave interaction of ocean surface gravity waves and peaking near 0.25Hz, is the largest amplitude, continuous (acceleration) vibration on earth in the seismic band from 0.0001 to 10Hz. Although microseisms have been studied extensively over the past seventy years, significant issues remain regarding their excitation and propagation. In a recent paper Bromirski et al (JGR, 2013) point out that there is an important distinction between microseisms generated in deep and shallow water. Most microseisms observed on continents are generated in shallow water near coastlines. Microseisms generated in deep water are observed on seafloor sensors but do not transition readily to continents. The Ocean Bottom Seismometer Augmentation to the Philippine Sea (OBSAPS) Experiment has provided a unique opportunity to study the excitation and propagation of microseism noise (from 0.05 to 1.0Hz) in the oceans by combining ocean bottom seismometer observations with co-located and simultaneous observations of the acoustic field in the ocean. The depth dependence of the acoustic field in the ocean can be used to distinguish between Rayleigh waves, acoustic and elastic pseudo-Rayleigh waves, and ocean acoustic modes as propagation mechanisms for microseism energy. (OBSAPS experiment was funded by ONR.)

I. Background - Pseudo-Rayleigh Waves (pRg)

In marine seismology the physics of wave propagation for the double frequency microseism band (0.1-0.5Hz) and typical ocean depths (100-6000m) spans the transition between solid earth seismology and ocean acoustics. At microseism frequencies, the water wavelengths are much longer than the thickness of soft sediment layers on the seafloor, the seafloor sediments can be ignored, and the bottom can be considered to consist of "hard rock", with a shear speed greater than the sound speed in the water. For laterally homogeneous models, the different phases generated by ocean surface gravity waves were reviewed by Ardhuin and Herbers (2012).

Many papers on microseism generation assume that, because storms at sea excite “Rayleigh waves” and because land arrays observe “Rayleigh waves”, then Rayleigh waves must easily propagate from the deep ocean onto land. Bromirski et al (2013) point out that storms at sea excite “pseudo-Rayleigh waves”, which are significantly different from “Rayleigh waves”, through the microseism band (0.1-0.5Hz) (Figure 1). For example, at frequencies above 0.2Hz and a water depth of 5000m “pseudo-Rayleigh waves” have considerable energy in the water column and propagate at water sound speeds (see Figure 2 for the frequency-depth trade-off of phase speed).

Pseudo-Rayleigh waves (below a fluid layer) do become indistinguishable from Rayleigh waves (on land) at low frequencies (below about 0.1Hz) where the thickness of the fluid layer becomes small compared to an acoustic wavelength. But for microseism studies the band of interest, 0.1-0.5Hz, spans the transition from free surface Rayleigh waves to propagating acoustic modes, acoustic pseudo-Rayleigh waves and direct water waves in the ocean as the ocean thickens with respect to frequency.

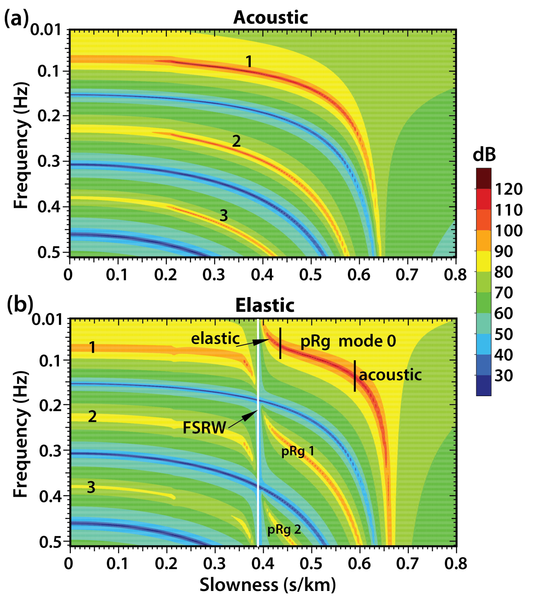

Figure 1: The magnitude of the wave fields in frequency-slowness space for a fluid layer (5 km thick with a sound speed of 1.520 km/s and a density of 1 kg/m^3) over (a) a fluid half-space (acoustic, zero shear modulus, with sound speed of 4.730 km/s and density of 3 kg/m^3), and (b) a solid half-space (elastic, compressional, and shear speeds of 4.730 and 2.800 km/s, respectively, free surface Rayleigh wave (FSRW) speed of 2.565 km/s, and a density of 3 kg/m^3). The FSRW slowness (0.39 s/km, white line) is the lower slowness bound for pseudo- Rayleigh wave (pRg) modes. Approximate boundaries where fundamental pRg mode 0 exhibits predominantly elastic or acoustic behavior are indicated by vertical black lines, with a transition region between. Acoustic modes 1, 2, and 3 are common to a and b. Although the fluid halfspace in a is unrealistic, comparison of these cases shows the effect of shear. Source and receivers are 0.050 km above the interface. These plots were computed using a seismo-acoustic fast-field algorithm (Schmidt, 1988). [Figure from Bromirski et al (2013).]

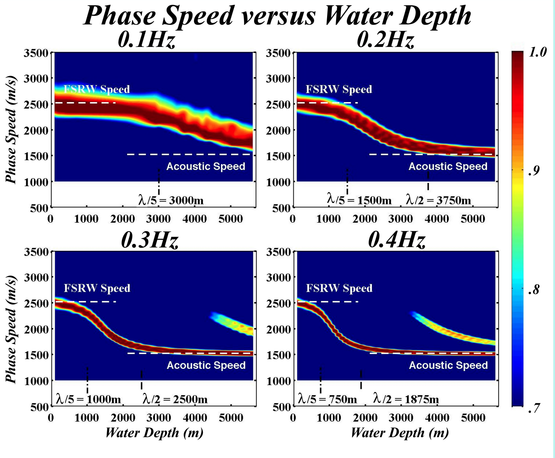

Figure 2: Relative wave field amplitude is shown as a function of phase speed and water depth for four frequencies spanning the microseism band. Spectral amplitudes (in dB) of the frequency-wave number field (as in Figures 13b and 13d below) are averaged over a 0.2 Hz band about the nominal frequency, converted to phase speed and normalized to the peak amplitude on the trace. Acoustic sound speed (1520 m/s) and FSRW speed (2518 m/s) are indicated by horizontal dashed lines. The spectral peak variation shows that, for frequencies in the microseism band, the dominant energy transitions from FSRW speeds to acoustic speeds as water depth increases. Phase-speed resolution, indicated by the width of the spectral peak, improves with increasing frequency. pRg mode 1 (see Figure 1) becomes evident between FSRW and acoustic phase speeds at deeper water depths as frequency increases. [Figure from Bromirski et al].